NASA TECHNICAL NOTE

NASA TN D-3930

NASA TN D-3930



# PHOTOMETRY OF SPECTROGRAMS OF THREE ARTIFICIAL METEORS

*by Gale A. Harvey*

*Langley Research Center*
*Langley Station, Hampton, Va.*

NATIONAL AERONAUTICS AND SPACE ADMINISTRATION • WASHINGTON, D. C. • MAY 1967

NASA TN D-3930

# PHOTOMETRY OF SPECTROGRAMS OF THREE ARTIFICIAL METEORS

By Gale A. Harvey

Langley Research Center
Langley Station, Hampton, Va.

NATIONAL AERONAUTICS AND SPACE ADMINISTRATION

For sale by the Clearinghouse for Federal Scientific and Technical Information
Springfield, Virginia 22151 – CFSTI price $3.00

# PHOTOMETRY OF SPECTROGRAMS OF THREE ARTIFICIAL METEORS

By Gale A. Harvey
Langley Research Center

## SUMMARY

Absolute spectral photometry has been performed on spectrograms of three artificial meteors. The meteors were a -3 magnitude, 10 km/s, 1.5-gram, iron dust-ball meteor at 48 kilometers' altitude; a -3 magnitude, 10.7 km/s, 1.5-gram iron dust-ball meteor at 68 kilometers' altitude; and a -1 magnitude, 9.5 km/s, 0.6-gram, solid iron meteor at 60 kilometers' altitude. Post-factum calibrations were used for most of the photometry.

The measurements are initial quantitative spectral data for meteors of known mass and composition and constitute initial quantitative meteoric spectral data in the near-ultraviolet region. The radiation recorded was atomic radiation from excited atoms of the artificial meteoroid material, and significant energies were associated with the iron meteoric radiation in the near-ultraviolet region.

## INTRODUCTION

Interest in meteor science has grown steadily in the last few years. Most of the interest has been centered on the concept of luminous efficiency – that is, the ratio of the instantaneous luminous energy radiated from a meteor to the instantaneous mass loss of the meteor. The luminous efficiency has been used extensively to compute meteoroid masses from photographic data, primarily in research on the meteoroid hazard to spacecraft. Verniani (ref. 1) and Ayers (ref. 2) discuss the methods used to investigate the luminous efficiency and the progress made in evaluating it over the years.

The meteor simulation project at the NASA Langley Research Center was established to measure the luminous and ionization efficiencies of artificial meteors of known mass, composition, density, and shape. Several artificial meteors have been produced, and all have been observed with optical instrumentation and some with low-frequency radar. Included in the ground-based optical equipment were several cameras designed to record the spectra of the reentry phenomena. The spectrograms can be used to study the physical and chemical characteristics of artificial meteoroids as they reenter the earth's atmosphere.

Absolute photometry of the spectrograms (the reduction of the spectral data to give absolute spectral irradiance) is of importance in determining the effect of chemical composition on luminous efficiency, in understanding the basic physical process of meteors (populations and distributions of the excited states), and in studying the anomalously large color indexes.

Good spectrograms of natural meteors are scarce, chiefly because of limitations of optical equipment, large distances from source to camera, and the extremely short effective exposure times ($10^{-2}$ s) caused by the high speed and short duration of meteors. Of the 259 spectrograms classified by Millman (ref. 3), only 16 contained more than 50 resolved lines. All the spectra lie in the visible or near-visible region of the electromagnetic spectrum. While a wavelength reduction has been performed on most of these meteor spectrograms and relative photometry on some, only 5 or 6 spectrograms have been reduced to obtain the absolute quantity of discrete radiation emitted by meteors. The results of the absolute photometry for spectrograms of two of these natural meteors were published by Cook and Millman in references 4 and 5. Analysis and interpretation of these data have been greatly restricted because the initial mass and composition of natural meteoroids are unknown. The physical processes that occur when a meteoroid enters the earth's atmosphere are so complex and the problems of observing or simulating meteors are of such magnitude that a theory to predict the spectral distribution of the meteor's irradiance has not been developed.

The acquisition of good quantitative spectral data from artificial meteors is a necessary step in the understanding of the meteoric processes. Such data will provide means to interpret the significance of the luminous and ionization efficiencies in the physical theory of meteors. The purpose of this research is (1) to exhibit the capability of measuring the spectra of dim artificial meteor entries and of extending the wavelength interval of the measurements, especially into the near ultraviolet, and (2) to analyze these data by the method of absolute photometry. The results of these efforts are presented in this report.

## DESCRIPTION OF THE EXPERIMENTS

Three experiments which resulted in the production of three dim artificial meteors are considered in this report. The experiment that produced each meteor is described, as well as the instrumentation used to observe the phenomena. The three dim artificial meteors are identified in this report by the rocket vehicle used in the experiment and the type of reentry body used to produce the meteor.

## Arcas-Margo, Iron Dust Ball

An Arcas-Margo meteor-simulation rocket was launched on the clear moonless night of September 26, 1963, at Wallops Island, Va. A shaped-charge accelerator carried as the payload by the rocket vehicle produced a low-density (approximately 0.05 $g/cm^3$) iron dust-ball meteoroid with a mass of 1.5 grams and a velocity of 10 km/s. The artificial meteoroid in turn produced a -3 magnitude meteor at a height of 48 kilometers. A description of the Arcas-Margo vehicle and the shaped-charge accelerator is given in reference 6, along with the integrated light curve and the luminous-efficiency data obtained from the experiment.

The Arcas-Margo meteor was photographed with several K-24 slitless spectrographs, which are f/2.5, 178-mm focal length, modified K-24 aerial cameras equipped with blazed objective diffraction gratings. These cameras, each equipped with a different diffraction grating ranging from 75 to 600 lines/mm, were located at Wallops Island, Va., and near Sandbridge, Va.

## Nike-Cajun, Iron Dust Ball

A Nike-Cajun meteor-simulation rocket was launched on the clear moonless night of November 6, 1964, at Wallops Island Va. A shaped-charge accelerator, identical to the one that produced the Arcas-Margo meteoroid, was carried as part of the payload by the rocket vehicle. The shaped-charge accelerator produced a low-density iron dust-ball meteoroid with a mass of 1.5 grams and a velocity of 10.7 km/s. The artificial meteoroid produced a -3 magnitude meteor of 0.1 s duration at a height of 68 kilometers.

The Nike-Cajun iron dust-ball meteor was photographed with the slitless spectrographs described below.

(1) A meniscus Schmidt camera, which is an f/0.83, 128-mm focal length, catadioptric camera with a $20^{\circ}$ field of view. The meniscus Schmidt, owned and operated by the Massachusetts Institute of Technology Lincoln Laboratory, is equipped with fused silica correcting lenses and a fused silica transmission objective diffraction grating with 150 lines/mm. This camera was located at Wallops Island, Va.

(2) A Super Schmidt camera, which is an f/0.65, 203-mm focal length, corrected, symmetrical, concentric Maksutov camera with a $57^{\circ}$ field of view. The Super Schmidt camera was equipped with an objective polystyrene mosaic prism and was located at Wallops Island, Va.

(3) Several K-24 spectrographs, which, as was mentioned earlier, are f/2.5, 178-mm focal length, modified K-24 aerial cameras equipped with objective diffraction gratings. The objective diffraction gratings ranged from 75 to 400 lines/mm. These cameras were located at Wallops Island, Va., and near Sandbridge, Va.

### Nike-Cajun, Solid Iron Pellet

The Nike-Cajun meteor-simulation rocket mentioned in the preceding section carried a second shaped-charge accelerator as the other part of the payload. The second shaped-charge accelerator produced a solid iron pellet-shaped meteoroid with a mass of 0.6 gram and a velocity of 9.5 km/s. The artificial meteoroid produced a -1 magnitude meteor of 0.4 s duration at a height of 60 kilometers.

Because of the proximity of the two Nike-Cajun meteors, they were both photographed with the same cameras and were therefore recorded on the same pieces of film.

## DATA REDUCTION

### Data

Arcas-Margo, iron dust ball.- Several spectrograms were obtained for the Arcas-Margo iron dust-ball meteor, but only the best spectrogram is presented and discussed in this report. The best spectrogram was obtained with a K-24 spectrograph with a diffraction grating of 400 lines/mm. An enlargement of this spectrogram is shown in figure 1.

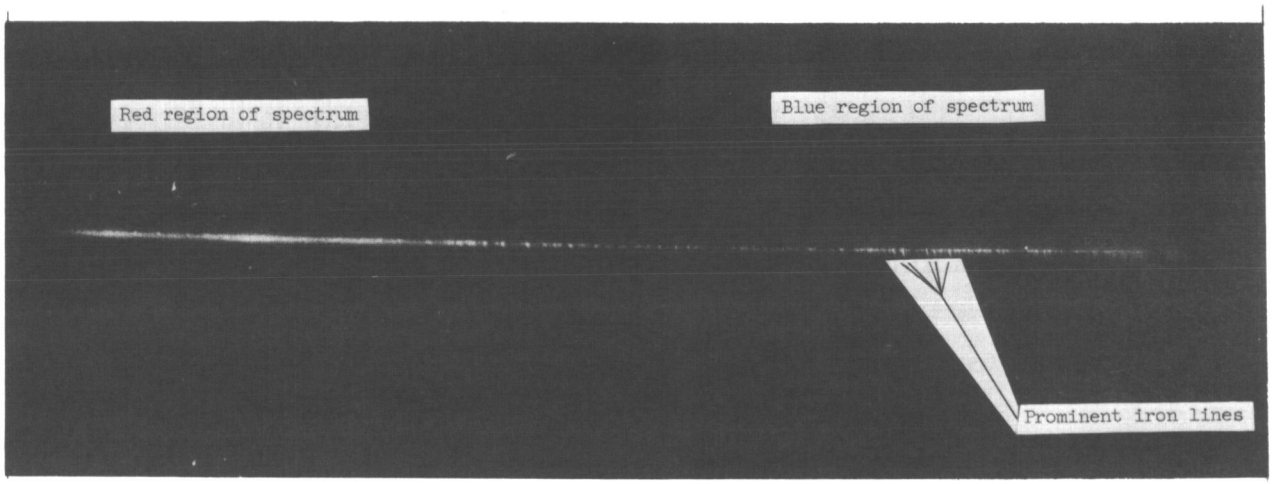


L-67-928

Figure 1.- Enlargement of spectrum from Arcas-Margo iron dust-ball meteor and shaped-charge detonation (K-24 spectrograph).

As a result of the low dispersion and resolution, most of the lines in the meteor spectrum are blended. The best quality data can be obtained in the 4000- to 5000-angstrom region because the blaze of the transmission diffraction grating was for the blue-green region of the spectrum and because the K-24 Aero-Ektar lens is not perfectly color corrected. The best focus during the artificial meteor event was at approximately 4300 angstroms. The increasing field angle is also responsible for some deterioration of the images in the red region of the spectrum.

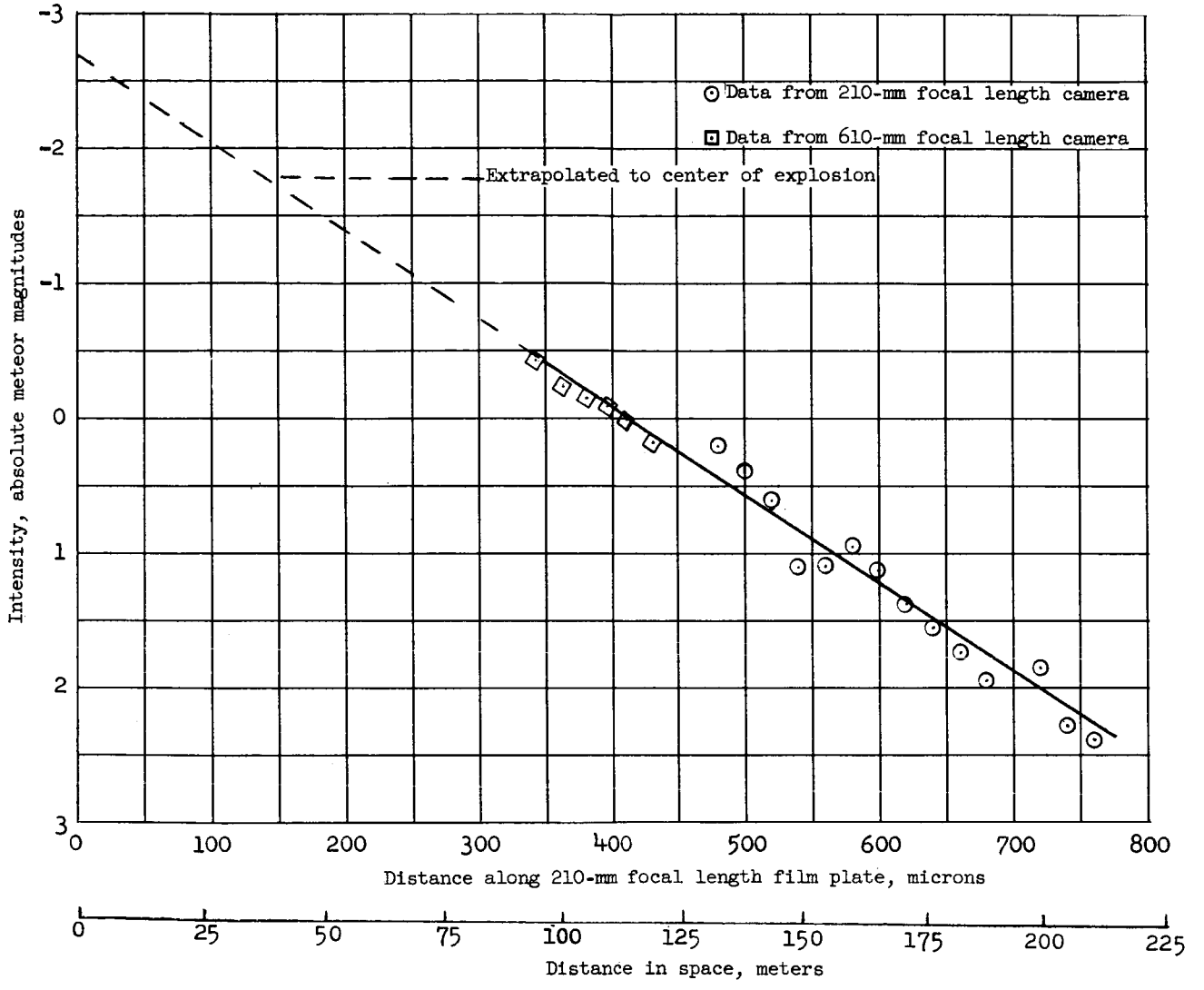


Figure 2.- Light curve of Arcas-Margo artificial iron dust-ball meteor for panchromatic film.

Most of the lines produced were less than 0.1 mm in length on the film, which corresponds to a distance of less than 60 meters in space along the meteor trail and could not be spatially resolved. The integrated light curve of this meteor, obtained from reference 6, shows that the light produced by the explosion of the shaped charge extended more than 60 meters from the point of explosion. (See fig. 2.) Therefore the spectrum of the radiation from the shaped-charge detonation is superimposed on the spectrum of the meteor. Nine of the iron lines in the blue region of the spectrum were strong enough to persist for a length slightly greater than 0.1 mm on the film. These nine lines are spatially resolved and parallel to the zero-order image, which shows that the meteor contributed at least in part to their formation. The nine iron lines were located at 4045.8, 4063.6, 4250.8, 4271.8, 4307.9, 4325.8, 4382.5, 4404.8, and 4415.1 angstroms. A number

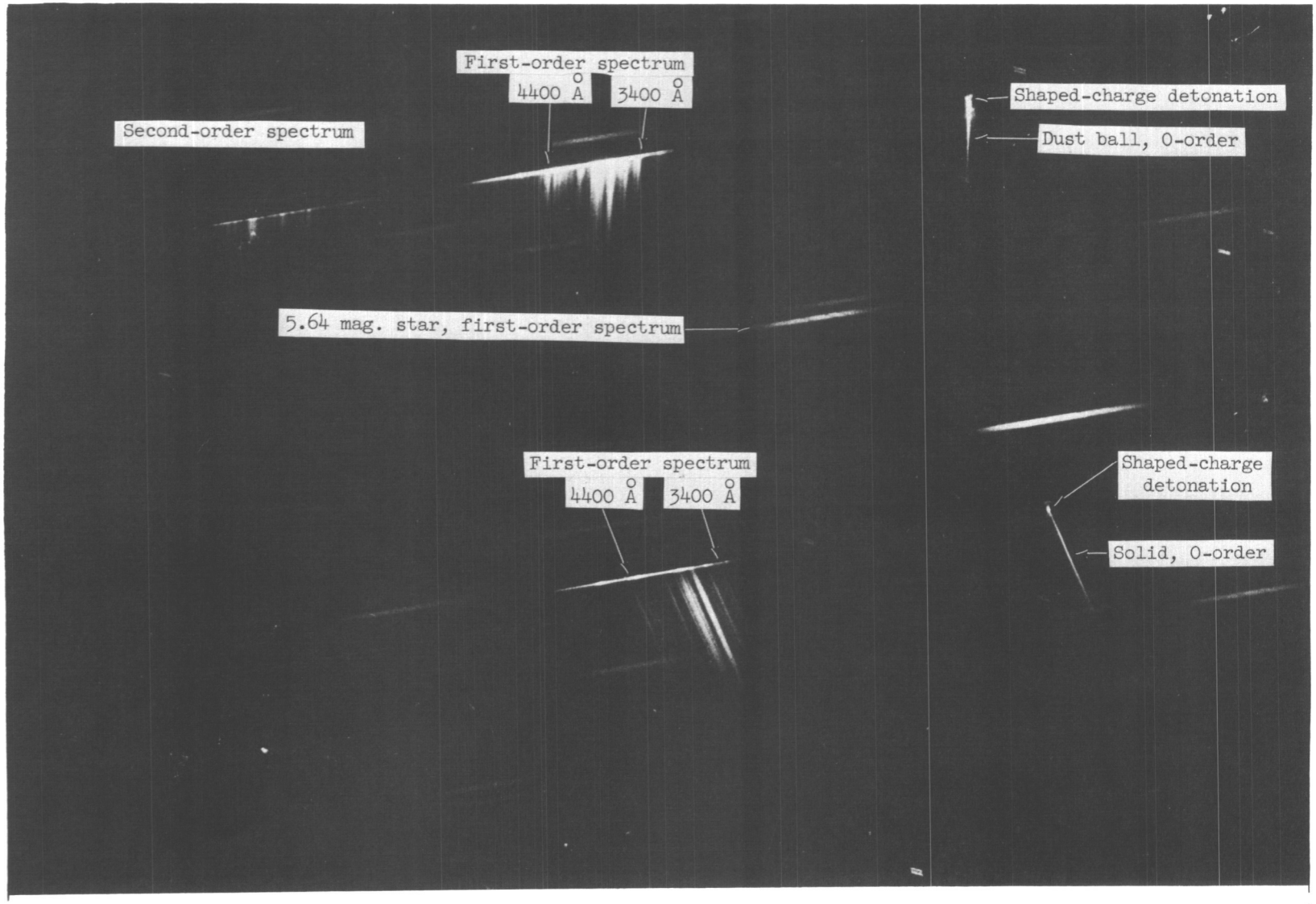


L-67-929

Figure 3.- Enlargement of near-ultraviolet spectrogram of Nike-Cajun iron dust-ball meteor and shaped-charge detonation, and of Nike-Cajun solid iron pellet meteor and shaped-charge detonation (meniscus Schmidt spectrograph).

of strong iron lines are present in the wavelength range from 4800 to 5500 angstroms, but deterioration of the image, caused primarily by chromatic aberration of the camera, does not allow positive spatial resolution of these iron lines.

Nike-Cajun, iron dust ball.- Several spectrograms were obtained for the Nike-Cajun iron dust-ball meteor, but only three are presented and discussed in this report, the spectrograms obtained with the meniscus Schmidt and the Super Schmidt, and the best one of the K-24 spectrograms. The spectrogram obtained with the meniscus Schmidt is shown in figure 3. The radiation recorded is in the 3200- to 4800-angstrom region. The lines in the first-order image are blended as a result of the low dispersion. The lines are of sufficient length to provide unquestionable spatial resolution, and hence time resolution, of the spectrum. The spectrum of the light produced by the detonation of the shaped charge is superimposed on the meteor spectrum only at the beginning of the meteor trail.

An enlargement of the spectrogram obtained with the Super Schmidt is shown in figure 4. Unfortunately the original data from the Super Schmidt spectrograph was lost, and only the data from a diapositive plate of the original negative was available. The radiation recorded was in the 3700- to 6500-angstrom region. A considerable amount of radiation was recorded in the red region of the spectrum. Most of the lines, which were blended because of the low dispersion, were long enough to provide spatial resolution of the spectrum. The spectrum of the shaped-charge detonation was superimposed on the meteor spectrum only at the beginning of the meteor trail.

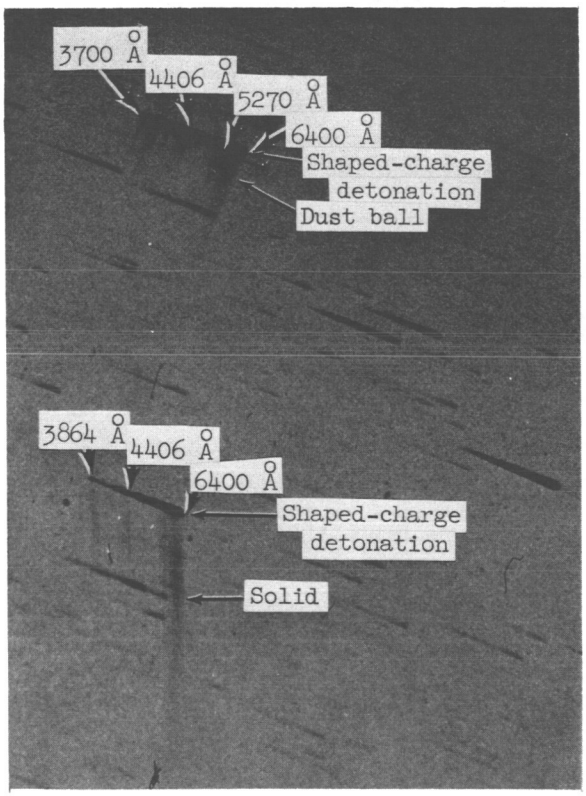


L-67-930

Figure 4.- Enlargement of Super Schmidt prismatic spectrogram of Nike-Cajun iron dust-ball meteor and shaped-charge detonation, and of Nike-Cajun solid iron pellet meteor and shaped-charge detonation.

The spectrogram obtained with the K-24 spectrograph is shown in figure 5. The K-24 spectrogram provides some spatial resolution, but because of the slower speed of this instrument the spatial resolution was not as good as that obtained with the Schmidt cameras.

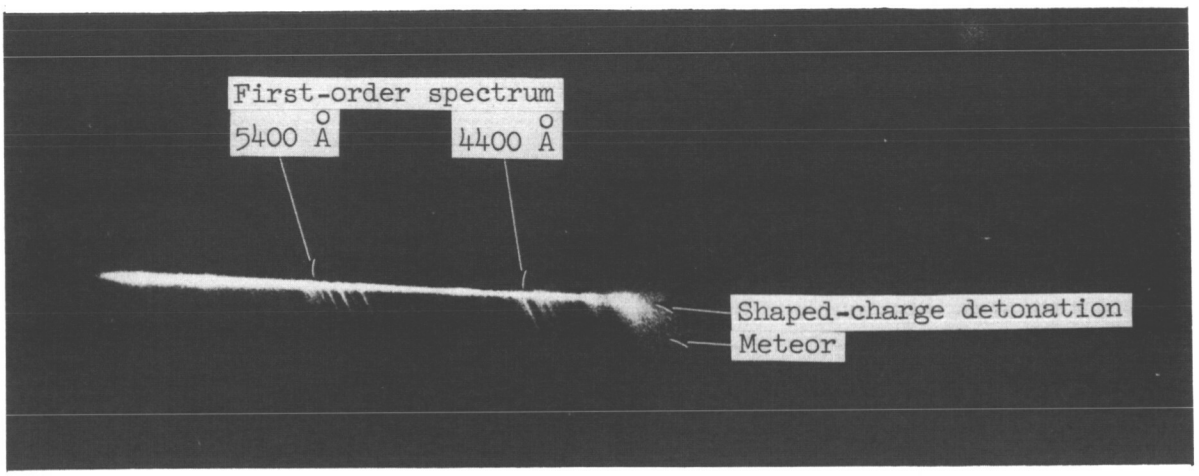


L-67-931

Figure 5.- Enlargement of visible spectrogram of Nike-Cajun iron dust-ball meteor and shaped-charge detonation (K-24 spectrograph).

Nike-Cajun, solid iron pellet.- Spectrograms of the Nike-Cajun solid iron meteor appeared on the same pieces of film as the Nike-Cajun iron dust-ball meteor. The meteor was too dim to be recorded by the slow K-24 spectrographs, but the spectrograms obtained with the meniscus Schmidt and the Super Schmidt will be discussed. Good spatial resolution was obtained on spectrograms from both the meniscus Schmidt (fig. 3) and the Super Schmidt (fig. 4). The spectrum of the shaped-charge detonation was not superimposed on the meteor spectrum in either spectrogram because the meteoroid did not begin to radiate brightly until it had cleared the area where the light from the shaped-charge detonation was produced.

## Photometry

The spectrograms were reduced to obtain the absolute spectral irradiance from the meteor at a distance of 100 km in a medium that transmits radiation perfectly; that is, the measured irradiance on the spectrogram was normalized to a distance of 100 km and corrected for atmospheric extinction. The analysis is a three-step procedure:

(1) The photometric optical density on the photographic negative of the spectrum is measured as a function of the wavelength

(2) The photometric optical density is related to the absolute irradiance incident on the spectrograph by means of a calibration curve obtained for the spectrograph

(3) The measurements are normalized; that is, the irradiance measurements for atmospheric extinction are corrected by measuring the irradiance of a standard star near the meteor at the time of the event and comparing the measured value with the known

irradiance from the star outside the earth's atmosphere, and then the irradiance is normalized to 100 km by using the inverse square law.

A fourth step is required in the case of the Arcas-Margo meteor, to determine what percentage of the irradiance was due to the meteor and what percentage was due to the detonation of the shaped charge.

The first step is rather straightforward and requires little explanation other than to say that the wavelength scale was constructed with the aid of the diffraction-grating equation and was adjusted to agree with a comparison-line spectrum or identified radiation of the spectrum being produced. The optical density was measured with a standard microdensitometer.

The second step of the analysis is discussed in more detail in the following paragraphs.

The density $D_\lambda$ of the image of a spectral line on a photographic plate used in a spectrograph is a function of the incident irradiance of that wavelength $H_\lambda$, the exposure time $t$, the grating transmission for that wavelength $G_\lambda$, the camera transmission for that wavelength $T(\theta)_\lambda$, which is also a function of the angle of incident light, and the response of the emulsion to radiation of that wavelength, which is called the film response or the film density function $S_\lambda$. Equation (1) is a functional equation expressing this relationship.

$$D_\lambda = f(H_\lambda, t, G_\lambda, T(\theta)_\lambda, S_\lambda) \tag{1}$$

The reciprocity law for a photographic emulsion states that the density resulting from light incident on the emulsion is a function of the exposure $Ht$ only, and not a function of $H$ and $t$ independently. The reciprocity law is valid for the panchromatic film used to photograph the meteor spectrum when the exposure time is between $10^{-5}$ s and $10^{-1}$ s. The effective exposure time for a meteor is approximately $10^{-2}$ s.

Because the function forms of $T(\theta)_\lambda$, $G_\lambda$, and $D_\lambda$ are complicated, they are not determined individually but are determined together by calibrating the film-camera-grating system as a single detection unit. Ideally the calibration is performed by recording the spectrum of a standard light source at several places on the same piece of film that will record the meteor event, just prior to the recording of the event. Various exposure times are used for the calibration spectra so that a range of exposures $H_\lambda t$ greater than that expected of the meteor event will be recorded. A densitometer trace is made of the blazed first-order images, and the values of transmission for different wavelengths are plotted against the log of the exposure to give the monochromatic H and D (Hurter and Driffield) curves. The optical path will not be the same for each image and each wavelength; therefore, off-axis light-loss corrections are applied to normalize all

the radiation to an on-axis light path. The exposure $H_\lambda t$ from the meteor can then be determined from the densitometer trace of the meteor spectrum, obtained in the first step of the analysis, and the H and D calibration curves. The exposure is then divided by the known effective exposure time to give the irradiance of the meteor. This irradiance must also be normalized to the on-axis light path. The effective exposure time is not the total duration of the meteor because the image of the meteor moves across the film; the effective exposure time is the time it takes the image to pass over one resolution area on the film.

The third step in the analysis, which is the correction for atmospheric extinction and range, is performed ideally by measuring the spectral irradiance of a standardized star recorded on the same piece of film that is used to record the spectrum of the meteor. The measurement is made by using a densitometer trace of the star spectrum and determining the corresponding exposure from the H and D calibration curves. The irradiance $H_\lambda$ found by dividing the exposure $H_\lambda t$ by the effective exposure time $t$ for the star must be corrected for reciprocity failure by means of the data in reference 7, because the effective exposure of a star is approximately 10 s, which is outside the exposure range for which the reciprocity law is valid. The difference between the spectral irradiance received at the camera from the star and the irradiance from this star outside the earth's atmosphere is the atmospheric extinction for the location, time, and sky area of the star and the meteor. Any difference between the zenith angles of the standardized star and the meteor is corrected for by using the zenith correction method in reference 8. A more complete discussion of absolute slitless spectrophotometry can be found in reference 9.

The advantage of placing the calibration images on the data film just prior to photographing the event is that possible errors arising from film differences and exposures having been taken at different times are eliminated. Furthermore the handling, storage, and exposure history of the calibration film and data film are identical, and image change or deterioration resulting from storage, heat, or other causes is automatically accounted for. A disadvantage is the possibility of having the meteor spectrum or a star spectrum fall on one of the calibration spectra. The use of separate pieces of film should not produce large errors if the pieces of film are from the same emulsion batch, especially if the calibration is made just prior to the recording of the meteor event and if the two films are then handled, stored, and processed together.

The advantage of having the standard-star spectrum needed for the calibration on the same piece of film as the data is to eliminate possible errors caused by a difference in location, time, and sky area between the data film and the calibration film. The disadvantage is the severe restrictions that would have to be placed on the trajectory of an artificial meteor to insure that it is near one of the few standardized stars. No large errors

should result if a second spectrograph, located near the data spectrograph, records the spectrum of a standardized star in the same area of the sky and at the same time as the meteor, provided of course that a good calibration procedure is followed for the second spectrograph.

## Calibrations

At the times the data in this report were obtained, sensitometers were not available to provide calibrations on all the data from a calibrated light source. Consequently, various means of calibration, some post-factum, were necessary to reduce the spectrograms. Absolute spectrophotometry was performed on three separate spectrograms: an Arcas-Margo 400 lines/mm K-24 spectrogram, a Nike-Cajun meniscus Schmidt spectrogram, and the Nike-Cajun K-24 spectrogram.

The spectral sensitometer discussed in reference 9 was used to obtain a post-factum calibration for the Arcas-Margo spectrogram approximately 1 year after the meteor experiment. The absolute sensitometric density step wedge was used to construct H and D curves at 100-angstrom intervals from 3700 to 6500 angstroms. Off-axis light-loss corrections (corrections for the variance of angle of incident light) for the K-24 camera were applied to each 100-angstrom interval.

The 400 lines/mm K-24 spectrogram on which the meteor was recorded did not contain a spectrum of a standardized star. However, a 75 lines/mm K-24 spectrograph, which was directed more northward at the time of the artificial-meteor event, recorded the spectrum of $\delta$ Ceti. Calibration of the meteor spectrogram was thus made possible by performing photometry on the $\delta$ Ceti spectrogram to obtain film, development, and atmospheric-extinction corrections.

The spectral energy distribution of $\delta$ Ceti, a B2 IV star, in the range 3750 to 5000 angstroms relative to the energy distribution of five B9 stars is given in reference 10. The intensity from 5000 to 6500 angstroms was also needed. The intensity distribution of $\gamma$ Orionis, a B2 III star, in the range 4500 to 10 320 angstroms relative to nine A0 stars is given in reference 11. The intensity distribution of $\delta$ Ceti was assumed to be the same as that of $\gamma$ Orionis in the region 5000 to 6500 angstroms. Allan F. Cook of the Smithsonian Institution Astrophysical Observatory provided the spectral energy distribution (standard curves) for the five B9 stars of reference 10 and the nine A0 stars of reference 11. The spectral class and stellar magnitude of $\delta$ Ceti is from reference 10 and the spectral class and stellar magnitude of $\gamma$ Orionis is from reference 12. As suggested by Cook, a value of $\log F_{5450} = -8.420$, where $F_{5450}$ is the irradiance outside the earth's atmosphere at 5450 angstroms in ergs/cm$^2$-Å-s, was used. Atmospheric extinction at $60^\circ$, the angle of the star $\delta$ Ceti from zenith at the time of the meteor, was

obtained from the photometry performed on the δ Ceti spectrogram. This was used to determine the coefficient of the secant function for atmospheric extinction, which in turn was used to obtain atmospheric extinction at the $40^{\circ}$ zenith angle of the meteor. A reciprocity-failure correction factor of 0.35 was applied to the meteor irradiance of this spectrogram. A range correction was made to normalize the range of the meteor to 100 kilometers.

The sensitometer described in reference 13 was used to obtain a post-factum calibration for the Nike-Cajun meniscus Schmidt spectrogram. This sensitometer provides a multichromatic density step wedge on film from which a multichromatic H and D curve can be obtained. Spectral photometry similar to that of reference 4 was performed on the spectrogram by determining the spectral irradiance corresponding to a particular density on the film. The first-order spectrum of a 5.64 magnitude A2 star was utilized for this purpose. The energy distribution of this star in the region 3400 to 6500 angstroms was assumed to be the same as that of $\alpha$ Cygni, an A2 Ia star, which is given in reference 14. The spectral class and magnitude of the 5.64 magnitude A2 star were obtained from reference 15.

The meteor and star spectra were within $5^{\circ}$ of the camera's optical axis and no off-axis corrections were applied (lens system is nearly concentric). No corrections were made for differences in zenith angle between the meteors and the star since the A2 star was at a zenith angle of $60.5^{\circ}$, the low-density iron meteor at a zenith angle of $59.5^{\circ}$, and the solid iron meteor at a zenith angle of $62^{\circ}$. Reciprocity-failure correction factors of 1 to 0.87 were applied to the meteor irradiance of this spectrogram. The meteor irradiance was normalized to a distance of 100 kilometers from the source.

The film calibration, not post factum, for the Nike-Cajun K-24 spectrograph was also obtained by using the sensitometer described in reference 13. The Nike-Cajun K-24 spectrogram contained the spectrum of $\epsilon$ Persei and the spectral photometry of this spectrogram is based upon the irradiance from this star. The intensity distribution of $\epsilon$ Persei, a B0.5 star, in the range 3750 to 6550 angstroms relative to the mean distribution of nine early-type stars is given in reference 11. A correction of 20 percent was applied to account for the difference in atmospheric extinction of $\epsilon$ Persei (zenith angle of $54.5^{\circ}$) and of the meteor (zenith angle of $59.5^{\circ}$). A reciprocity-failure correction factor of 0.37 was applied to the meteor irradiance of this spectrogram. The meteor irradiance was normalized to a distance of 100 kilometers from the source.

## RESULTS

### Arcas-Margo Meteor

The radiation recorded on the Arcas-Margo spectrogram (fig. 1), as previously mentioned, resulted from two different events: the meteor and the detonation of the shaped charge. It is desirable, therefore, that the contribution of radiation from each event be determined. The spatially resolved meteor trail recorded on the negatives which were used to obtain the light curve prove that some of the radiation is from the meteor. Each spectral line would be expected to decrease monotonically with distance from the origin, that is, from the shaped-charge detonation, as does the light curve of figure 2. The shape of the light curve of figure 2 agrees closely with the shape of the aluminum low-density-meteor light curve and the shape of a predicted light curve for low-density meteors of reference 16. It would be expected, then, that the strongest lines would be spatially resolved and that weaker lines would not be resolved. This is exactly the case in the blue region of the spectrum.

The spectrogram of the Arcas-Margo low-density iron meteor was compared with spectrograms of the Nike-Cajun low-density iron meteor. Examination of the Nike-Cajun spectrograms revealed that about half of the atomic radiation was from the shaped-charge detonation and about half was from the low-density iron meteor. About one-fourth of the red radiation was iron-oxide radiation from the meteor and three-fourths was iron-oxide and unidentified radiation from the shaped-charge detonation. It is assumed that the same percentages are valid for the Arcas-Margo low-density meteor. The spectral irradiance from the Arcas-Margo meteor and shaped-charge detonation is presented in figure 6.

Most of the radiation attributed to the Arcas-Margo meteor is atomic-line radiation. The wavelengths of this atomic radiation are presented in table I. The entries in column 1 are wavelengths read from a 50× densitometer tracing of the spectrogram by means of a constructed wavelength scale. Column 2 contains rounded-off values of wavelengths from reference 17. Column 3 lists the element which emitted the radiation and column 4 lists the arc intensity for the radiation as given in reference 15. Column 5 lists the multiplet of the radiation as determined from reference 18.

Because of the low dispersion and blending of the lines, two aids were used in identification of the wavelength and source of the radiation: (1) an 8-angstrom-per-millimeter dc arc spectrogram on which the resolution was about 0.5 angstrom and (2) the intensities listed in reference 17. Table I contains 243 lines of iron in 99 multiplets, and 15 lines of manganese in 8 multiplets. These results are reasonable in light of the fact that a spectrochemical analysis gave a chemical composition of 97.8 percent or more iron, 0.5 to 0.9 percent manganese, 0.1 to 0.9 percent chromium, 0.05 to 0.09 percent copper and

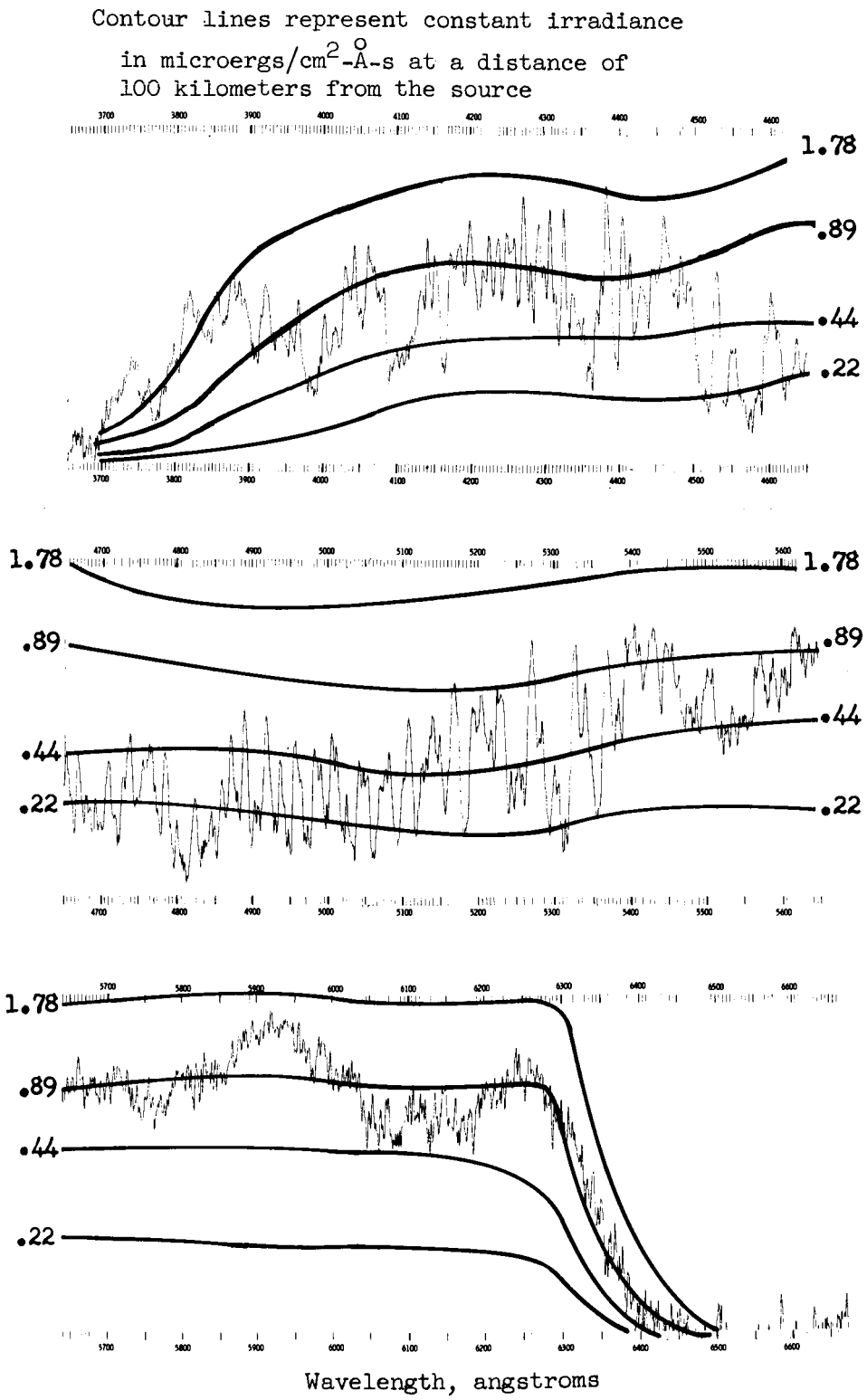


Figure 6.- Spectral irradiance from Arcas-Margo artificial iron dust-ball meteor and shaped-charge detonation.

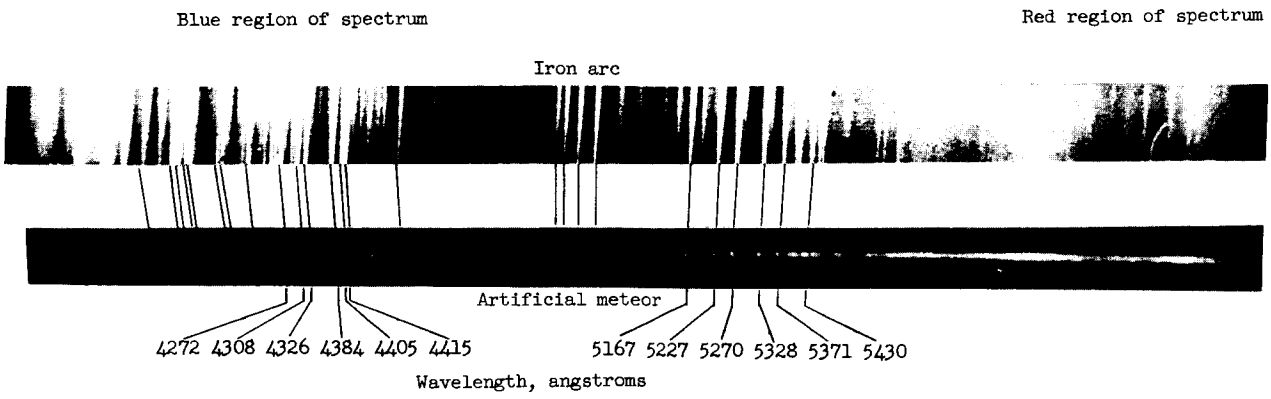


Figure 7.- Enlargements of iron-arc spectrogram and Arcas-Margo artificial-meteor spectrogram. L-67-932

nickel, 0.01 to 0.09 percent zinc, and minute traces of cobalt, tin, molybdenum, and zirconium, with 0.072 percent carbon, 0.012 percent phosphorus, and 0.023 percent sulfur for the meehanite cast iron.

A spectrogram of radiation from an iron (of the same material as produced the meteor) dc arc was recorded with the same camera that recorded the artificial meteor spectrum on Kodak Royal X panchromatic film. This spectrogram (fig. 7) shows that the emissions from the two sources of excitation were not greatly different.

## Nike-Cajun Iron Dust Ball

Meteoric radiation from the Nike-Cajun iron dust-ball meteor was recorded by three different spectrographs. Radiation in the interval from 3200 to 6400 angstroms was recorded. Enlargements of the Nike-Cajun iron dust-ball spectrograms are shown in figures 3, 4, and 5. Absolute spectral irradiance from this meteor is presented in figures 8 and 9. The light curve of the meteor is presented in figure 10. The spectral irradiance of figures 8 and 9 corresponds to times of 0.04 second and 0.015 second on the light curve of figure 10.

From figures 3, 4, and 5 it is seen that radiation is emitted in the near-ultraviolet, blue, green, and red regions of the spectrum. Although the radiation is at discrete wavelengths, it is not heavily concentrated in any one region of the spectrum. Thus a broadband detection system in one of these wavelength regions would not, on the basis of these spectrograms, give a result very greatly different from a broadband detection system in another of these regions, provided all the measurements are based on a nearly white continuous standard. The color index of a meteor is a measure of the difference between measurements, in different broad wavelength regions, of the same source when compared

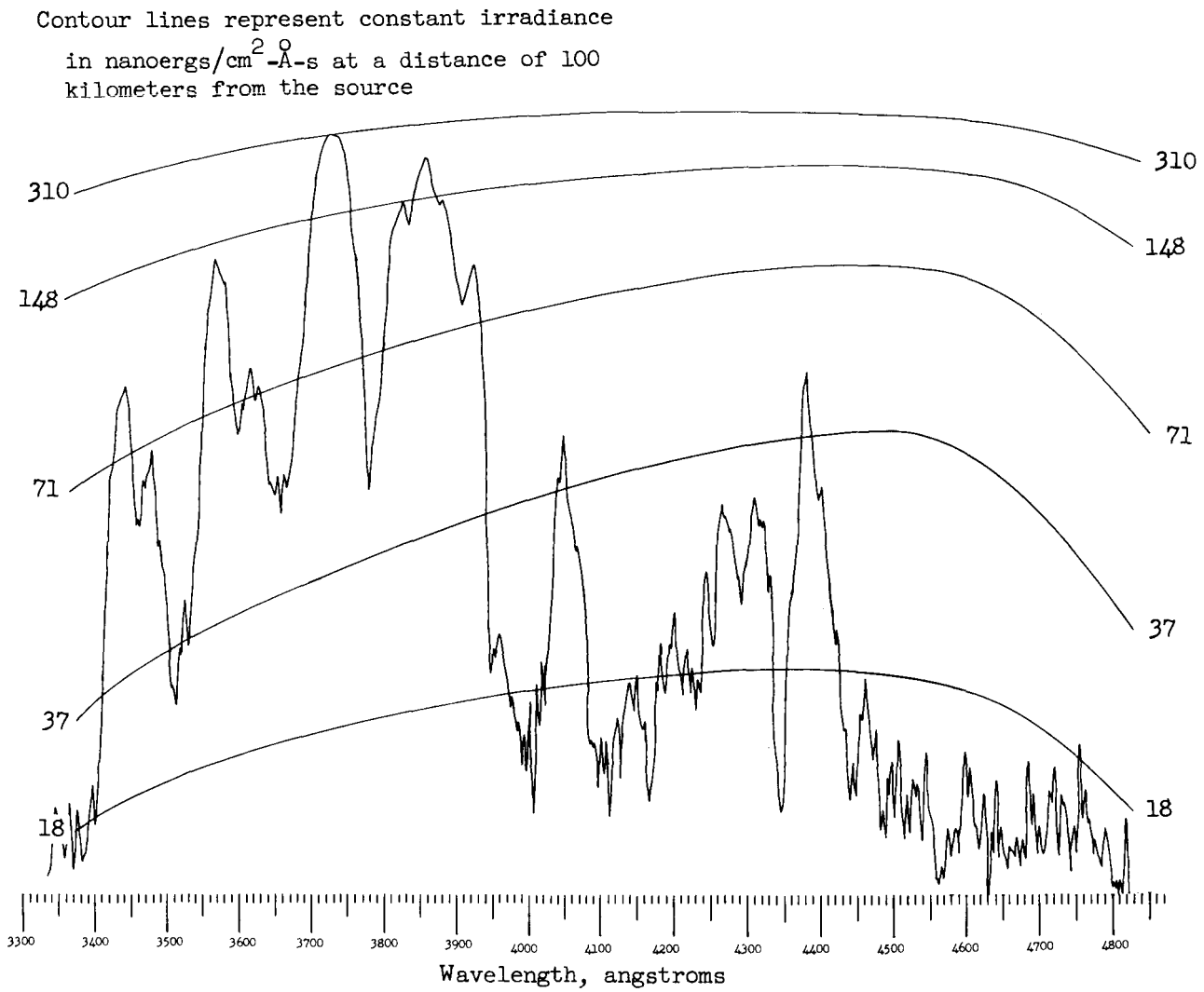


Figure 8.- Irradiance from Nike-Cajun artificial iron dust-ball meteor in the near-ultraviolet region at 0.04 second (meniscus Schmidt spectrogram).

against a common standard (AO stars). The Nike-Cajun low-density spectrograms do not support the large (>10) color index factors which are sometimes used to correlate data in meteor research. (See ref. 19.)

Most of the radiation from the Nike-Cajun iron dust-ball meteor is atomic-line radiation. The wavelengths identified on the meniscus Schmidt spectrogram (fig. 3) are presented in table II, the wavelengths identified on the K-24 spectrogram are presented in table III, and the wavelengths of radiation on the Super Schmidt diapositive is presented in table IV.

Figure 4, the enlargement of the Super Schmidt prismatic spectrogram, shows considerable red radiation from both the Nike-Cajun meteors. Although the dispersion

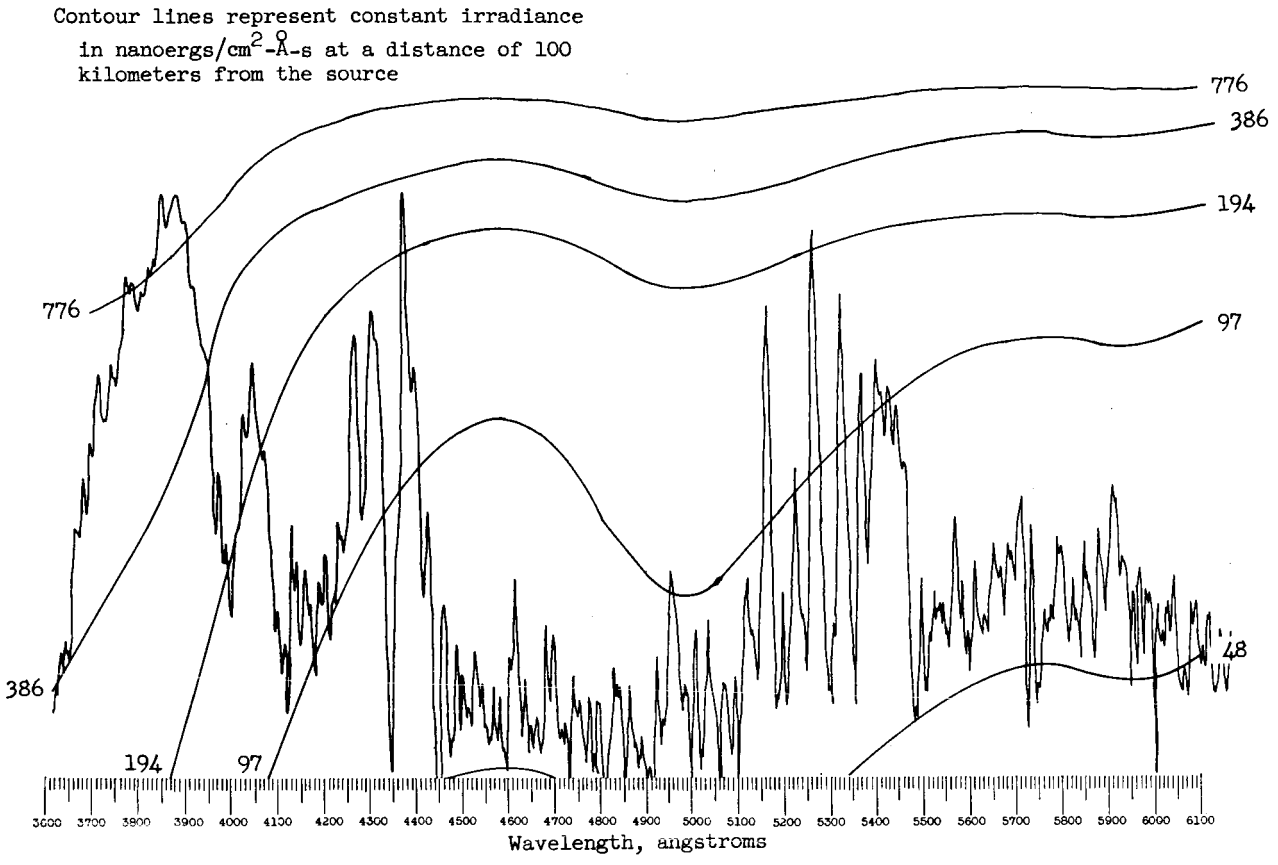


Figure 9.- Irradiance from Nike-Cajun artificial iron dust-ball meteor in the visible region at 0.015 second (K-24 spectrogram).

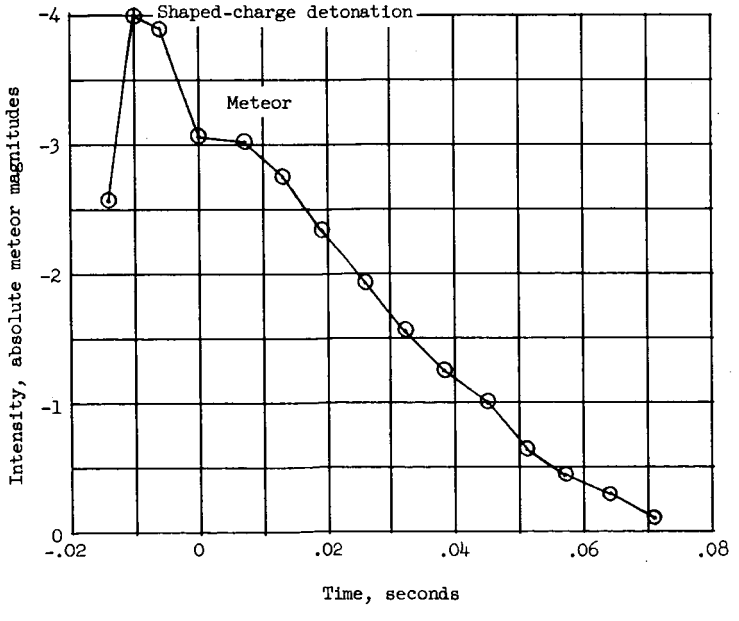


Figure 10.- Light curve of Nike-Cajun artificial iron dust-ball meteor for panchromatic film.

and resolution of the Super Schmidt diapositive plate is not good enough to allow positive identification of this radiation, the absence of strong iron lines in this region (see fig. 7), the apparently diffuse or unresolved character of the radiation on the prismatic spectrogram; and the similarity of the meteor spectrum to that of an iron arc indicate that most of this radiation is from iron oxide.

## Nike-Cajun Solid Iron Pellet

Meteoric radiation from the Nike-Cajun solid iron pellet was recorded by two different spectrographs. Radiation in the interval from 3400 to 6400 angstroms was recorded. Absolute spectral irradiance from the iron pellet meteor in the near-ultraviolet and blue regions is presented in figure 11. The spectral irradiance of figure 11 corresponds to a time of 0.088 second on the light curve of figure 12.

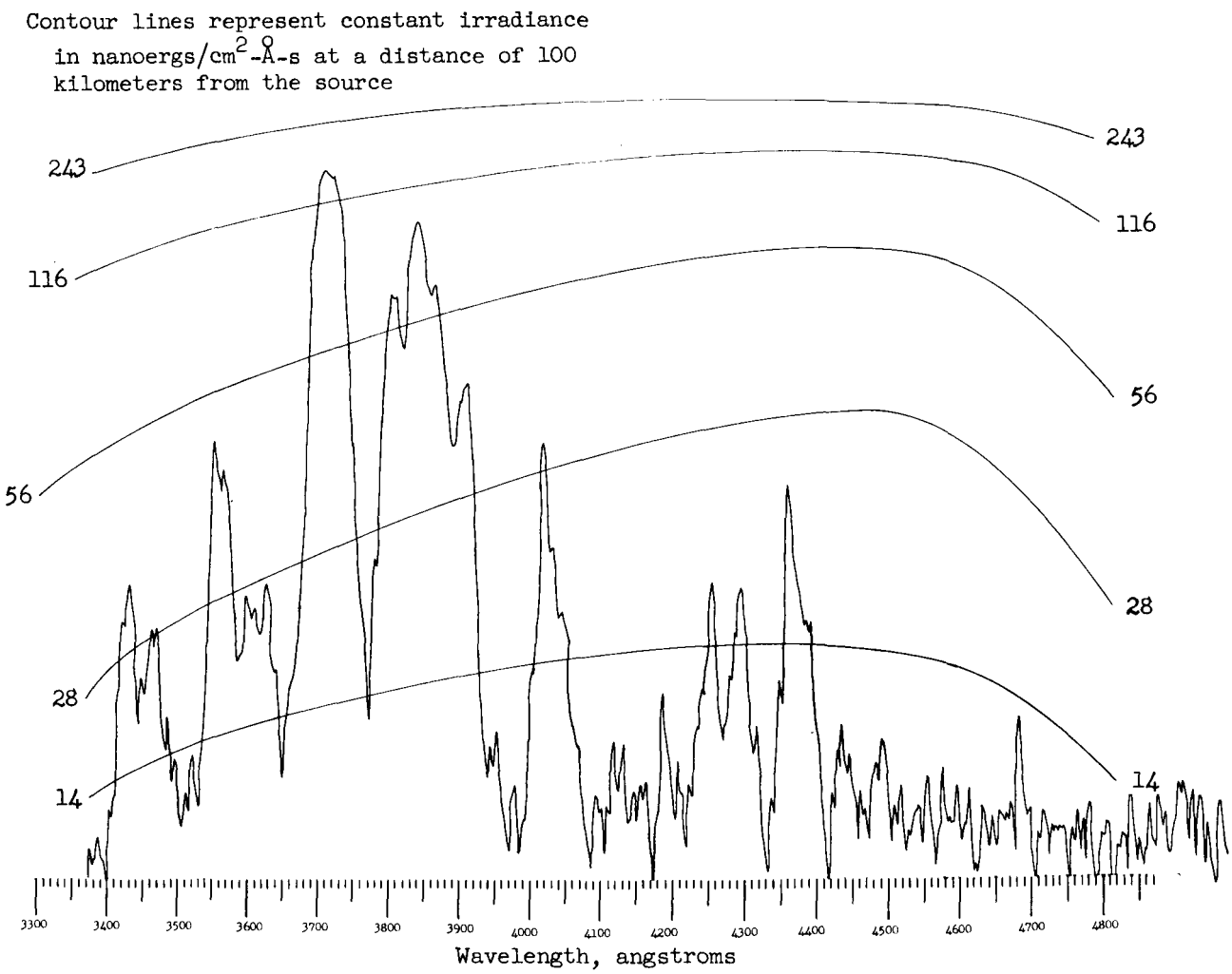


Figure 11.- Irradiance from Nike-Cajun artificial solid iron pellet meteor in the near-ultraviolet region at 0.088 second (meniscus Schmidt spectrogram).

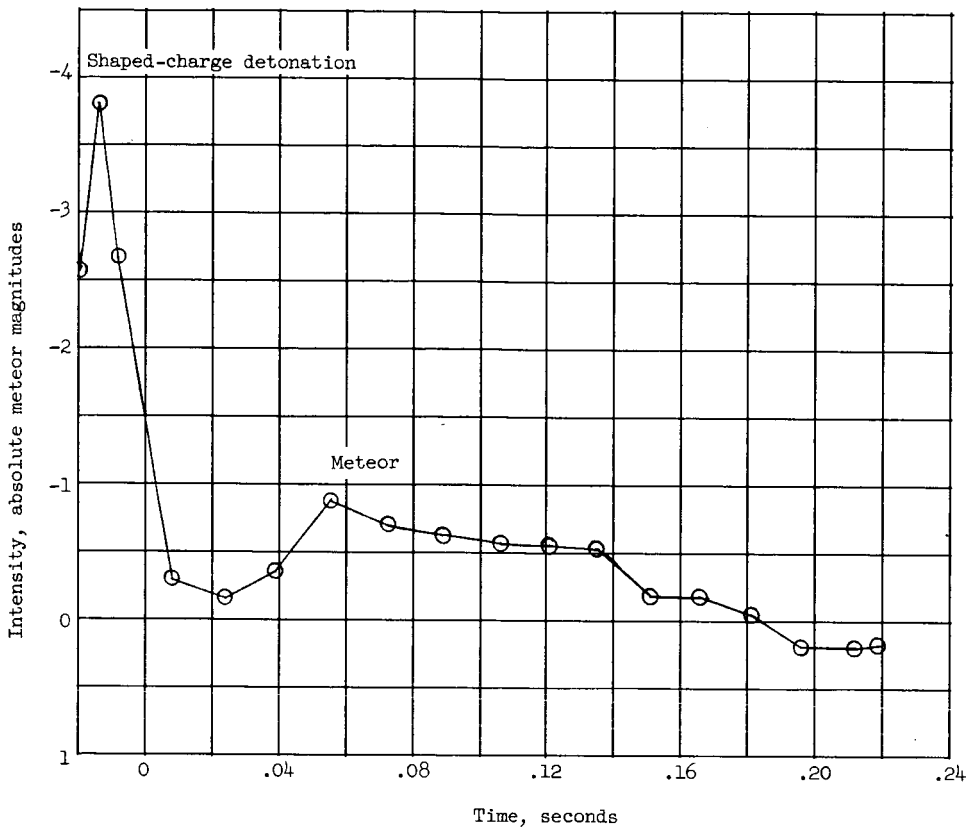


Figure 12.- Light curve of Nike-Cajun artificial solid iron pellet meteor for panchromatic film.

Again, most of the meteor radiation is atomic-line radiation. The wavelengths identified on the meniscus Schmidt spectrogram are presented in table V and the radiation identified on the Super Schmidt diapositive is presented in table VI.

The errors resulting from not having good calibration images placed on the data film just prior to or immediately after photographing the event (i.e., errors arising from different film batches and processing at different times) are difficult to evaluate. The error resulting from the absence of a suitable standardized star in the immediate reentry area, which requires the introduction of another spectrogram in the calibration and reduction, is also difficult to evaluate. A measure of the accuracy of the photometry can be obtained by comparing the irradiance from the Nike-Cajun dust-ball meteor as reduced from the meniscus Schmidt spectrogram with the irradiance reduced from the K-24 spectrogram at the same wavelength. The irradiance at 4230 and 4280 angstroms at 0.04 second (fig. 8) is approximately 30 nanoergs/cm$^2$-Å-s. The irradiance at 4230 and 4280 angstroms at 0.015 second (fig. 9) is approximately 170 nanoergs/cm$^2$-Å-s. From the light curve of figure 10 we find that the meteor was 1.43 magnitudes or a factor of 3.73 more intense at 0.015 second than at 0.04 second. Thus the irradiance from figure 9 at

0.04 second would be approximately 45.5 nanoergs/cm$^2$-Å-s. Therefore, including errors of time resolution, the two reductions agree within 52 percent.

## DISCUSSION

Absolute spectral photometry has been performed on spectrograms of three artificial meteors. This photometry represents crude measurements for all three meteor spectra. Absolute spectral photometry of slitless spectrograms of the kind reduced here is possible with an accuracy of 20 percent, as shown in reference 9, if careful field calibrations are employed. However, post-factum and multichromatic calibrations, as discussed in the section entitled "Calibrations," had to be employed in photometry, and as a result larger errors, +52 percent for example, are representative of the accuracy of the present measurements. However, the measurements are believed to be significant for several reasons. They constitute the most sensitive (i.e., of the faintest meteors) quantitative spectral data of the meteoric processes yet obtained. The measurements are the only quantitative spectral data for meteors of known mass and chemical composition, and they constitute the only known quantitative data in the near-ultraviolet region. More than 250 lines of atomic radiation were identified in a slitless meteor spectrogram. All three of the meteor spectrograms are well in the top of Millman's classification scheme for meteor spectrograms (ref. 3).

The photometry of the three artificial meteors indicates that major effort is needed in the areas of extending the accuracy and precision of the measurements, extending the wavelength interval, and upgrading field technique. In view of the energies in the near-ultraviolet region in the meteor processes, as evidenced by the meniscus Schmidt spectrogram, an extension of the wavelength interval of good photometry down to 3200 angstroms is very much needed. The absence of stellar standards of spectral irradiance in this wavelength region makes the extension difficult.

Most of the radiation attributed to these artificial meteors is atomic radiation from atoms of meteoric material, and important contributions of iron oxide radiation exist in the red region of the spectrum. No air radiation was identified.

Preliminary work with a dc-arc-excited source indicates that the spectrum of a low-velocity artificial iron meteor is not greatly different from dc iron arc spectra.

The absolute spectral irradiance data in this report does not support the large color indexes reported in the literature.

The spectrograms reduced are from 3 to 5 meteor magnitudes dimmer than those of references (4) and (5). Meteor spectrograms from high-performance (f/1 or faster with high transmission glasses) spectrographs with optimum operation and film development can be used to obtain quantitative spectral data of +1 magnitude meteors. Further

advances in the field of meteor spectroscopy will probably result in the use of image orthocon, image intensifier, and similar photoelectric sensors to increase the sensitivity of slitless spectrographs.

Integrated light data have been the primary tool of the meteor scientists, and recently measurements of ionization produced by meteors have greatly aided those scientists. However, neither of these data systems can compare with the information content of high-quality meteor spectrograms. With the expected advances in slitless spectroscopy which should allow good absolute spectral irradiance measurements of meteors of +1 and fainter absolute meteor magnitude, a wealth of information on the physical processes of meteors will become available.

Langley Research Center,
National Aeronautics and Space Administration,
Langley Station, Hampton, Va., December 14, 1966,
709-06-00-01-23.

## REFERENCES


1. Verniani, Franco: On the Luminous Efficiency of Meteors. Spec. Rept. No. 145, Smithsonian Inst. Astrophys. Obs., Feb. 17, 1964.

2. Ayers, Wendell G.: Luminous Efficiency of an Artificial Meteor at 11.9 Kilometers per Second. NASA TN D-2931, 1965.

3. Millman, Peter M.: A General Survey of Meteor Spectra. Smithsonian Contrib. Astrophys., vol. 7, 1963, pp. 119-127.

4. Cook, Allan F.; and Millman, Peter M.: Photometric Analysis of a Spectrogram of a Perseid Meteor. Astrophys. J., vol. 121, no. 1, Jan. 1955, pp. 250-270.

5. Millman, Peter M; and Cook, Allan F.: Photometric Analysis of a Spectrogram of a Very Slow Meteor. Astrophys. J., vol. 130, no. 2, Sept. 1959, pp. 648-662.

6. Harvey, Gale A.: Photographic Observations of a Low-Density Iron Artificial Meteoroid. NASA TN D-3420, 1966.

7. Anon.: Kodak Tech Bits, No. 3, Eastman Kodak Co., 1964.

8. Blanco, V. M.; and McCuskey, S. W.: Basic Physics of the Solar System. Addison-Wesley Pub. Co., Inc., c.1961.

9. Harvey, Gale A.: A Method of Slitless Absolute Spectral Photometry. NASA TN D-3765, 1967.

10. Bonsack, Walter K.; and Stock, Jurgen: Photoelectric Spectrophotometry. II. Monochromatic Colors of O-, B-, and A-Type Stars. Astrophys. J., vol. 126, no. 1, July 1957, pp. 99-112.

11. Kienle, Von H.; Strassl, H.; and Wempe, J.: Die relative Energieverteilung im kontinuierlichen Spektrum von 36 Fundamentalsternen. Z. Astrophys., Bd. 16, Nr. 4, 1938, pp. 201-275.

12. Northcott, Ruth J., ed.: The Observer's Handbook 1964. Roy. Astron. Soc. Can.

13. Wyckoff, Charles W.; and Edgerton, Harold E.: Xenon Electronic Flash Sensitometer. J. SMPTE, vol. 66, Aug. 1957, pp. 474-479.

14. Code, A. D.: Stellar Energy Distribution. Stellar Atmospheres, Jesse L. Greenstein, ed., Univ. of Chicago Press, c.1960, pp. 50-87.

15. Boss, Benjamin: General Catalogue of 33342 Stars for the Epoch 1950. Pub. No. 468, vol. III, Carnegie Inst. of Washington, 1937.

16. McCrosky, Richard E.: Observations of Simulated Meteors. Smithsonian Contrib. Astrophys., vol. 5, no. 4, 1961, pp. 29-36.

17. Harrison, George R., compiler: Massachusetts Institute of Technology Wavelength Tables. John Wiley & Sons, Inc., [1960].

18. Moore, Charlotte E.: A Multiplet Table of Astrophysical Interest – Revised Edition. NBS Tech. Note 36 (PB 151395), U.S. Dept. Com., Nov. 1959.

19. Davis, John: Photoelectric Meteor Observations and the Colour Indices and Visual Magnitudes of Meteors. Monthly Notices, Roy Astron. Soc., vol. 126, no. 5, 1963, pp. 445-467.

TABLE I.- VISIBLE RADIATION FROM ARCAS-MARGO IRON DUST-BALL METEOR

| Wavelength measured | Wavelength identified | Element | Arc intensity | Multiplet | Wavelength measured | Wavelength identified | Element | Arc intensity | Multiplet |
|---|---|---|---|---|---|---|---|---|---|
| 3733 | 3734.9 | Fe | 1000r | 21 | 3927 | 3927.9 | Fe | 500 | 4 |
| 3739 | 3737.1 | Fe | 1000r | 5 | 3930 | 3930.3 | Fe | 600 | 4 |
| 3748 | 3749.5 | Fe | 1000r | 21 | 3938 | 3935.8 | Fe | 100 | 362 |
| 3753 | 3753.6 | Fe | 150 | 73 | 3942 | 3940.9 | Fe | 150 | 20 |
| 3765 | 3763.8 | Fe | 500 | 21 | 3947 | 3948.8 | Fe | 150 | 604 |
| 3770 | 3767.2 | Fe | 500 | 21 | 3952 | 3951.2 | Fe | 150 | 661 |
| 3791 | 3787.9 | Fe | 500 | 21 | 3965 | 3963.1 | Fe | 125 | 562 |
| 3792 | 3790.1 | Fe | 200 | 22 | 3971 | 3969.3 | Fe | 600 | 43 |
| 3798 | 3795.0 | Fe | 500 | 21 | 3979 | 3977.7 | Fe | 300 | 72 |
| | 3798.5 | Fe | 400 | 21 | 3987 | 3984.0 | Fe | 200 | 277 |
| | 3799.5 | Fe | 400 | 21 | 4006 | 4005.2 | Fe | 250 | 43 |
| 3803 | 3805.5 | Fe | 400 | 608 | 4010 | 4009.7 | Fe | 120 | 72 |
| 3807 | 3806.3 | Fe | 200 | 607 | 4018 | 4021.9 | Fe | 200 | 278 |
| 3812 | 3813.0 | Fe | 400 | 22 | 4023 | 4024.7 | Fe | 120 | 560 |
| 3816 | 3815.8 | Fe | 700 | 45 | 4033 | 4030.5 | Fe | 120 | 560 |
| 3820 | 3820.4 | Fe | 800 | 20 | | 4030.8 | Mn | 500r | 2 |
| 3825 | 3824.4 | Fe | 150 | 4 | 4034 | 4033.1 | Mn | 400r | 2 |
| 3827 | 3825.9 | Fe | 500 | 20 | 4035 | 4034.5 | Mn | 250r | 2 |
| 3828 | 3827.8 | Fe | 200 | 45 | 4042 | 4040.6 | Fe | 20 | 655 |
| 3834 | 3834.2 | Fe | 400 | 20 | 4048 | 4045.5 | Fe | 400 | 43 |
| 3842 | 3840.4 | Fe | 400 | 20 | 4055 | 4055.0 | Mn | 80 | 5 |
| | 3841.1 | Fe | 500 | 45 | 4065 | 4063.6 | Fe | 400 | 43 |
| 3846 | 3846.8 | Fe | 125 | 664 | 4074 | 4071.7 | Fe | 300 | 43 |
| 3851 | 3850.0 | Fe | 500 | 20 | 4080 | 4079.8 | Fe | 80 | 359 |
| 3860 | 3856.4 | Fe | 500 | 4 | 4086 | 4084.5 | Fe | 120 | 698 |
| | 3859.9 | Fe | 1000r | 4 | 4087 | 4085.3 | Fe | 100 | 559 |
| 3864 | 3865.5 | Fe | 600 | 20 | 4095 | 4096.0 | Fe | 80 | 217 |
| 3870 | 3872.5 | Fe | 300 | 20 | 4098 | 4098.2 | Fe | 100 | 558 |
| 3876 | 3878.0 | Fe | 400 | 20 | 4102 | 4103.0 | Mn | 100 | Unlisted |
| | 3878.6 | Fe | 300R | 4 | 4105 | 4105.4 | Mn | 50 | 47 |
| 3882 | 3885.5 | Fe | 100 | 124 | 4109 | 4109.8 | Fe | 120 | 357 |
| 3883 | 3886.3 | Fe | 600 | 4 | | 4110.9 | Mn | 80r | 37 |
| 3885 | 3888.8 | Fe | 40 | 488 | | 4110.9 | Mn | 80r | 47 |
| 3893 | 3893.9 | Fe | 10 | 175 | 4116 | 4118.5 | Fe | 200 | 801 |
| 3895 | 3895.7 | Fe | 400 | 4 | 4120 | 4121.8 | Fe | 100 | 356 |
| 3898 | 3897.9 | Fe | 100 | 280 | 4128 | 4127.6 | Fe | 100 | 357 |
| 3901 | 3899.7 | Fe | 500 | 4 | 4133 | 4132.1 | Fe | 300 | 43 |
| 3904 | 3903.0 | Fe | 500 | 45 | 4136 | 4134.7 | Fe | 150 | 357 |
| 3907 | 3906.5 | Fe | 300 | 4 | 4144 | 4143.4 | Fe | 200 | 523 |
| 3910 | 3909.8 | Fe | 40 | 364 | | 4143.9 | Fe | 400 | 43 |
| 3912 | 3913.6 | Fe | 100 | 120 | 4156 | 4153.9 | Fe | 120 | 695 |
| 3916 | 3917.2 | Fe | 150 | 20 | | 4154.5 | Fe | 100 | 355 |
| 3920 | 3920.3 | Fe | 500 | 4 | | 4154.8 | Fe | 100 | 694 |
| 3922 | 3922.9 | Fe | 600 | 4 | 4157 | 4156.8 | Fe | 100 | 354 |

TABLE I.- VISIBLE RADIATION FROM ARCAS-MARGO IRON DUST-BALL METEOR – Continued

| Wavelength measured | Wavelength identified | Element | Arc intensity | Multiplet | Wavelength measured | Wavelength identified | Element | Arc intensity | Multiplet |
|---|---|---|---|---|---|---|---|---|---|
| 4177 | 4174.9 | Fe | 100 | 19 | 4435 | 4433.2 | Fe | 150 | 830 |
| | 4175.6 | Fe | 100 | 354 | 4442 | 4442.3 | Fe | 400 | 68 |
| | 4176.6 | Fe | 100 | 695 | 4443 | 4443.2 | Fe | 200 | 350 |
| | 4177.6 | Fe | 100 | 18 | 4447 | 4447.7 | Fe | 200 | 68 |
| 4185 | 4184.9 | Fe | 100 | 355 | 4454 | 4454.4 | Fe | 200 | 350 |
| 4187 | 4187.0 | Fe | 250 | 152 | 4461 | 4459.1 | Fe | 400 | 68 |
| | 4187.8 | Fe | 200 | 152 | 4465 | 4466.6 | Fe | 500 | 350 |
| 4192 | 4191.4 | Fe | 200 | 152 | 4477 | 4476.0 | Fe | 500 | 350 |
| 4200 | 4198.3 | Fe | 250 | 152 | 4482 | 4482.2 | Fe | 150 | 2 |
| | 4199.1 | Fe | 300 | 522 | | 4482.3 | Fe | 150 | 68 |
| 4203 | 4202.0 | Fe | 400 | 42 | 4485 | 4484.2 | Fe | 125 | 828 |
| 4209 | 4208.6 | Fe | 100 | 689, 696 | 4491 | 4489.7 | Fe | 100 | 2 |
| | 4210.4 | Fe | 300 | 152 | 4494 | 4494.6 | Fe | 400 | 68 |
| 4218 | 4219.4 | Fe | 250 | 800 | 4510 | 4508.3 | Fe | 40 | 38 |
| 4221 | 4222.2 | Fe | 200 | 152 | 4529 | 4528.6 | Fe | 600 | 68 |
| 4228 | 4227.4 | Fe | 300 | 693 | 4550 | 4547.9 | Fe | 200 | 755 |
| 4238 | 4235.9 | Fe | 300 | 152 | | 4549.5 | Fe | 100 | 38 |
| 4241 | 4238.8 | Fe | 200 | 693 | 4555 | 4556.1 | Fe | 150 | 410 |
| 4251 | 4250.1 | Fe | 250 | 152 | | 4556.1 | Fe | 150 | 820 |
| | 4250.8 | Fe | 400 | 42 | | 4556.1 | Fe | 150 | 974 |
| 4261 | 4260.5 | Fe | 400 | 152 | 4581 | 4583.8 | Fe | 150 | 38 |
| 4273 | 4271.2 | Fe | 400 | 152 | 4594 | 4592.7 | Fe | 200 | 39 |
| | 4271.8 | Fe | 1000 | 42 | 4600 | 4598.1 | Fe | 50 | 554 |
| 4284 | 4282.4 | Fe | 600 | 71 | 4603 | 4602.9 | Fe | 300 | 39 |
| 4292 | 4291.5 | Fe | 125 | 3 | 4612 | 4611.3 | Fe | 200 | 826 |
| | 4291.5 | Fe | 125 | 31 | 4631 | 4632.9 | Fe | 70 | 39 |
| 4394 | 4294.1 | Fe | 700 | 41 | 4637 | 4637.5 | Fe | 100 | 554 |
| 4300 | 4298.0 | Fe | 100 | 520 | | 4638.0 | Fe | 80 | 822 |
| | 4299.2 | Fe | 500 | 152 | 4649 | 4647.4 | Fe | 125 | 409 |
| 4307 | 4307.9 | Fe | 1000R | 42 | 4655 | 4654.5 | Fe | 20 | 38 |
| 4315 | 4315.1 | Fe | 500 | 71 | 4668 | 4667.5 | Fe | 150 | 822 |
| 4326 | 4325.8 | Fe | 1000 | 42 | 4669 | 4668.1 | Fe | 125 | 554 |
| 4337 | 4337.0 | Fe | 400 | 41 | 4679 | 4678.9 | Fe | 150 | 821 |
| 4340 | 4344.0 | Fe | 100 | 6 | 4690 | 4691.4 | Fe | 80 | 409 |
| 4347 | 4346.6 | Fe | 50 | 598 | 4708 | 4707.3 | Fe | 100 | 554 |
| 4353 | 4352.7 | Fe | 300 | 71 | 4710 | 4709.7 | Mn | 150 | 21 |
| 4370 | 4369.8 | Fe | 200 | 518 | 4734 | Unidentified | | | |
| 4376 | 4375.9 | Fe | 500 | 2 | 4738 | 4736.8 | Fe | 125 | 554 |
| 4384 | 4383.5 | Fe | 1000 | 41 | 4739 | 4739.1 | Mn | 150 | 21 |
| 4397 | 4395.3 | Fe | 80 | 828 | 4754 | 4754.0 | Mn | 400 | 16 |
| 4405 | 4404.8 | Fe | 1000 | 41 | 4757 | Unidentified | | | |
| 4415 | 4415.1 | Fe | 600 | 41 | 4764 | 4762.4 | Mn | 100 | 21 |
| 4428 | 4427.3 | Fe | 500 | 2 | 4766 | 4766.4 | Mn | 80 | 21 |
| 4432 | 4430.6 | Fe | 200 | 68 | 4784 | 4786.8 | Fe | 150 | 467 |

TABLE I.- VISIBLE RADIATION FROM ARCAS-MARGO IRON DUST-BALL METEOR – *Concluded*

| Wavelength measured | Wavelength identified | Element | Arc intensity | Multiplet | Wavelength measured | Wavelength identified | Element | Arc intensity | Multiplet |
|---|---|---|---|---|---|---|---|---|---|
| 4787 | 4789.7 | Fe | 100 | 753 | 5204 | 5202.3 | Fe | 300 | 66 |
| | 4791.2 | Fe | 200 | 633 | 5205 | 5204.6 | Fe | 125 | 1 |
| 4820 | 4821.0 | Fe | 200h | Unlisted | 5216 | 5216.3 | Fe | 300 | 36 |
| 4825 | 4823.5 | Mn | 400 | 16 | 5227 | 5227.2 | Fe | 400 | 37 |
| 4859 | 4859.7 | Fe | 150 | 318 | 5251 | 5250.7 | Fe | 150 | 66 |
| 4871 | 4871.3 | Fe | 200 | 318 | 5253 | 5253.5 | Fe | 70 | 553 |
| 4872 | 4872.1 | Fe | 100 | 318 | | 5266.6 | Fe | 500 | 383 |
| 4877 | 4878.2 | Fe | 80 | 318 | 5268 | 5269.5 | Fe | 800 | 15 |
| 4890 | 4890.8 | Fe | 100 | 318 | | 5270.4 | Fe | 400 | 37 |
| | 4891.5 | Fe | 70 | 318 | 5279 | 5281.8 | Fe | 300 | 383 |
| 4904 | 4903.3 | Fe | 500 | 318 | 5281 | 5283.6 | Fe | 400 | 553 |
| 4908 | 4909.4 | Fe | 50 | 985 | 5298 | Unidentified | | | |
| 4917 | 4919.0 | Fe | 300 | 318 | 5302 | 5302.3 | Fe | 300 | 553 |
| 4919 | 4920.5 | Fe | 500 | 318 | | 5324.2 | Fe | 400 | 553 |
| 4925 | 4925.3 | Fe | 1000R | 1065 | 5326 | 5328.0 | Fe | 400 | 15 |
| 4938 | 4938.8 | Fe | 300 | 318 | | 5328.5 | Fe | 150 | 37 |
| 4957 | 4957.3 | Fe | 100 | 318 | 5339 | 5341.1 | Mn | 200 | 4 |
| | 4957.6 | Fe | 300 | 318 | | 5367.5 | Fe | 200h | 1146 |
| 4967 | 4966.1 | Fe | 300 | 687 | 5168 | 5370.0 | Fe | 15h | 1146 |
| 4984 | 4983.3 | Fe | 100h | 1067 | | 5371.5 | Fe | 700 | 15 |
| | 4983.9 | Fe | 200h | 1066 | 5382 | 5383.4 | Fe | 400h | 1146 |
| 5008 | Unidentified | | | | | 5397.1 | Fe | 400 | 15 |
| 5014 | 5015.0 | Fe | 500 | 965 | 5400 | 5400.5 | Fe | 125 | 1145 |
| 5027 | 5027.1 | Fe | 60 | 1065 | 5405 | 5404.1 | Fe | 300 | 1165 |
| | 5027.2 | Fe | 60 | 883 | | 5405.8 | Fe | 400 | 15 |
| 5043 | 5041.8 | Fe | 300 | 36 | 5411 | 5410.9 | Fe | 200 | 1165 |
| 5049 | 5049.8 | Fe | 400 | 114 | 5426 | 5424.1 | Fe | 400 | 1146 |
| 5051 | 5051.6 | Fe | 200 | 16 | 5430 | 5429.7 | Fe | 500 | 15 |
| 5072 | 5068.8 | Fe | 400 | 383 | 5433 | 5434.5 | Fe | 300 | 15 |
| 5077 | 5079.2 | Fe | 100 | 66 | 5445 | 5446.9 | Fe | 300 | 15 |
| | 5079.9 | Fe | 100 | 16 | 5449 | Unidentified | | | |
| 5082 | 5083.3 | Fe | 200 | 16 | 5455 | 5455.6 | Fe | 300 | 15 |
| 5108 | 5107.5 | Fe | 100 | 16 | 5463 | 5463.0 | Fe | 50 | 1163 |
| | 5110.4 | Fe | 300 | 1 | | 5463.3 | Fe | 100 | 1163 |
| 5125 | 5123.7 | Fe | 200 | 16 | 5475 | 5473.9 | Fe | 100 | 1062 |
| 5135 | 5133.7 | Fe | 200h | 1092 | | 5474.9 | Fe | 100 | Unlisted |
| 5139 | 5137.4 | Fe | 200h | 1090 | 5498 | 5497.5 | Fe | 150 | 15 |
| 5148 | 5150.8 | Fe | 150 | 16 | | 5501.5 | Fe | 150 | 15 |
| 5167 | 5162.3 | Fe | 300h | 1089 | 5505 | 5506.8 | Fe | 150 | 15 |
| | 5167.5 | Fe | 700 | 37 | 5524 | Unidentified | | | |
| | 5171.6 | Fe | 300 | 36 | 5570 | 5569.6 | Fe | 300 | 686 |
| 5192 | 5191.5 | Fe | 400 | 383 | | 5572.8 | Fe | 300 | 686 |
| 5194 | 5192.4 | Fe | 400 | 383 | 5586 | 5586.8 | Fe | 400 | 686 |
| 5198 | 5198.7 | Fe | 80 | 66 | 5705 | 5709.4 | Fe | 100h | 686 |

TABLE II.- NEAR-ULTRAVIOLET RADIATION FROM NIKE-CAJUN IRON DUST-BALL METEOR

| Wavelength measured | Wavelength identified | Element | Arc intensity | Multiplet | Wavelength measured | Wavelength identified | Element | Arc intensity | Multiplet |
|---|---|---|---|---|---|---|---|---|---|
| 3424 | 3424.3 | Fe | 200 | 81 | 3885 | 3886.3 | Fe | 600 | 4 |
| 3441 | 3440.6 | Fe | 500 | 6 | 3926 | 3927.9 | Fe | 500 | 4 |
| | 3441.0 | Fe | 300 | 6 | | 3930.3 | Fe | 600 | 4 |
| | 3443.9 | Fe | 400 | 6 | 3951 | 3948.8 | Fe | 150 | 604 |
| | 3445.2 | Fe | 300 | 81 | | 3950.0 | Fe | 150 | 72 |
| 3470 | 3465.9 | Fe | 500 | 6 | | 3951.2 | Fe | 150 | 661 |
| 3480 | 3475.4 | Fe | 400 | 6 | 3960 | 3956.5 | Fe | 100 | 605 |
| | 3476.7 | Fe | 300 | 6 | | 3956.7 | Fe | 150 | 278 |
| 3494 | 3490.6 | Fe | 400 | 6 | 3975 | 3977.7 | Fe | 300 | 72 |
| 3526 | 3521.3 | Fe | 300 | 24 | 4001 | 3997.4 | Fe | 300 | 278 |
| 3572 | 3554.9 | Fe | 400 | 154 | | 3998.0 | Fe | 150 | 276 |
| | 3556.9 | Fe | 300 | 327 | 4011 | 4013.8 | Fe | 200 | 486 |
| | 3558.5 | Fe | 400 | 24 | | 4014.5 | Fe | 200 | 802 |
| | 3565.4 | Fe | 400 | 24 | 4050 | 4045.8 | Fe | 400 | 43 |
| | 3570.1 | Fe | 300 | 24 | 4060 | 4063.6 | Fe | 400 | 43 |
| | 3572.0 | Fe | 100 | 321 | 4123 | 4118.6 | Fe | 200 | 801 |
| 3586 | 3581.2 | Fe | 1000 | 23 | | 4121.8 | Fe | 100 | 356 |
| 3605 | 3608.9 | Fe | 500 | 23 | 4140 | 4143.9 | Fe | 400 | 43 |
| 3616 | 3618.8 | Fe | 400 | 23 | 4184 | 4181.8 | Fe | 200 | 763 |
| 3630 | 3631.5 | Fe | 500 | 23 | 4203 | 4202.0 | Fe | 400 | 42 |
| 3654 | 3647.8 | Fe | 500 | 23 | 4219 | 4219.4 | Fe | 250 | 800 |
| | 3651.5 | Fe | 300 | 295 | 4246 | 4250.1 | Fe | 250 | 152 |
| 3685 | 3679.9 | Fe | 500 | 5 | | 4250.8 | Fe | 400 | 42 |
| | 3682.2 | Fe | 400 | 772 | 4270 | 4260.5 | Fe | 400 | 152 |
| | 3683.1 | Fe | 200 | 5 | | 4271.2 | Fe | 400 | 152 |
| | 3684.1 | Fe | 300 | 292 | | 4271.8 | Fe | 1000 | 42 |
| 3735 | 3705.6 | Fe | 700 | 5 | 4280 | 4282.4 | Fe | 600 | 71 |
| | 3709.3 | Fe | 600 | 21 | 4291 | 4294.1 | Fe | 700 | 41 |
| | 3719.9 | Fe | 1000 | 5 | 4313 | 4307.9 | Fe | 1000 | 42 |
| | 3722.6 | Fe | 500 | 5 | | 4315.1 | Fe | 500 | 71 |
| | 3733.3 | Fe | 400 | 5 | | 4325.8 | Fe | 1000 | 42 |
| | 3734.9 | Fe | 1000 | 21 | 4336 | 4337.0 | Fe | 400 | 41 |
| | 3737.1 | Fe | 1000 | 5 | 4358 | 4352.7 | Fe | 300 | 71 |
| | 3745.6 | Fe | 500 | 5 | 4386 | 4383.6 | Fe | 1000 | 41 |
| | 3748.3 | Fe | 500 | 5 | 4406 | 4404.8 | Fe | 1000 | 41 |
| | 3749.5 | Fe | 1000 | 21 | 4425 | 4422.6 | Fe | 300 | 350 |
| | 3758.2 | Fe | 700 | 21 | | 4427.3 | Fe | 500 | 2 |
| 3787 | 3787.9 | Fe | 500 | 21 | 4465 | 4459.1 | Fe | 400 | 68 |
| 3828 | 3820.4 | Fe | 800 | 20 | | 4461.6 | Fe | 300 | 2 |
| | 3825.9 | Fe | 500 | 20 | | 4466.6 | Fe | 500 | 2 |
| | 3834.2 | Fe | 400 | 20 | 4479 | 4476.0 | Fe | 500 | 350 |
| 3861 | 3856.4 | Fe | 500 | 4 | | | | | |
| | 3859.9 | Fe | 1000 | 4 | | | | | |
| | 3865.5 | Fe | 600 | 20 | | | | | |

TABLE III.- VISIBLE RADIATION FROM NIKE-CAJUN IRON DUST-BALL METEOR

| Wavelength measured | Wavelength identified | Element | Arc intensity | Multiplet | Wavelength measured | Wavelength identified | Element | Arc intensity | Multiplet |
|---|---|---|---|---|---|---|---|---|---|
| 3860 | 3850.0 | Fe | 500 | 20 | 4310 | 4294.1 | Fe | 700 | 41 |
| | 3856.4 | Fe | 500 | 4 | | 4299.3 | Fe | 500 | 152 |
| | 3859.9 | Fe | 1000 | 4 | | 4307.9 | Fe | 1000 | 42 |
| 3890 | 3878.0 | Fe | 400 | 20 | 4320 | 4315.1 | Fe | 500 | 71 |
| | 3878.6 | Fe | 300 | 175 | | 4325.8 | Fe | 1000 | 42 |
| | 3886.3 | Fe | 600 | 4 | 4380 | 4375.9 | Fe | 500 | 2 |
| | 3895.7 | Fe | 400 | 4 | | 4383.6 | Fe | 1000 | 41 |
| | 3899.7 | Fe | 500 | 4 | 4401 | 4404.8 | Fe | 1000 | 41 |
| | 3903.0 | Fe | 500 | 45 | 4429 | 4422.6 | Fe | 300 | 350 |
| 3928 | 3927.9 | Fe | 500 | 4 | | 4427.3 | Fe | 500 | 2 |
| | 3930.0 | Fe | 600 | 4 | Not observed | 4925.3 | Fe | 1000 | 1065 |
| 3950 | 3948.1 | Fe | 125 | 562 | 4958 | 4957.6 | Fe | 300 | 318 |
| | 3948.8 | Fe | 150 | 604 | 5126 | 5123.7 | Fe | 200 | 16 |
| | 3950.0 | Fe | 150 | 72 | | 5125.1 | Fe | 100 | 1110 |
| | 3951.2 | Fe | 150 | 661 | | 5127.4 | Fe | 100 | 16 |
| 3978 | 3977.7 | Fe | 300 | 72 | 5170 | 5167.5 | Fe | 700 | 37 |
| 4017 | 4013.8 | Fe | 200 | 485 | | 5171.6 | Fe | 300 | 36 |
| | 4014.5 | Fe | 200 | 802 | 5230 | 5227.2 | Fe | 400 | 37 |
| | 4021.9 | Fe | 200 | 278 | | 5232.9 | Fe | 800 | 383 |
| 4030 | 4030.8 | Mn | 500 | 2 | 5270 | 5263.3 | Fe | 300 | 553 |
| | 4030.5 | Fe | 120 | 560 | | 5266.6 | Fe | 500 | 383 |
| 4052 | 4045.8 | Fe | 400 | 43 | | 5269.5 | Fe | 800 | 15 |
| | 4063.6 | Fe | 400 | 43 | | 5270.4 | Fe | 400 | 37 |
| 4080 | 4084.5 | Fe | 120 | 698 | 5329 | 5324.2 | Fe | 400 | 553 |
| | 4085.3 | Fe | 100 | 559 | | 5328.0 | Fe | 400 | 15 |
| 4100 | 4098.2 | Fe | 100 | 152 | 5374 | 5371.5 | Fe | 700 | 15 |
| 4135 | 4132.1 | Fe | 300 | 43 | 5406 | 5404.2 | Fe | 300 | 1165 |
| 4145 | 4143.8 | Fe | 400 | 43 | | 5405.8 | Fe | 400 | 15 |
| 4209 | 4208.6 | Fe | 100 | 689, 696 | 5414 | 5415.2 | Fe | 500 | 1165 |
| | 4210.4 | Fe | 300 | 152 | 5433 | 5429.7 | Fe | 500 | 15 |
| | 4213.6 | Fe | 100 | 355 | | 5434.5 | Fe | 300 | 15 |
| 4234 | 4233.6 | Fe | 250 | 152 | 5450 | 5446.9 | Fe | 300 | 15 |
| | 4235.9 | Fe | 300 | 152 | | 5455.6 | Fe | 300 | 15 |
| 4272 | 4260.5 | Fe | 400 | 152 | 5465 | 5463.3 | Fe | 100 | 1163 |
| | 4271.2 | Fe | 400 | 152 | 5572 | 5569.2 | Fe | 300 | 686 |
| | 4271.8 | Fe | 1000 | 48 | | 5572.8 | Fe | 300 | 686 |
| | 4282.4 | Fe | 600 | 71 | | | | | |

TABLE IV.- RADIATION FROM NIKE-CAJUN IRON DUST-BALL METEOR RECORDED ON SUPER SCHMIDT SPECTROGRAM

| Wavelength identified | Element | Arc intensity | Multiplet | Wavelength identified | Element | Arc intensity | Multiplet |
|---|---|---|---|---|---|---|---|
| 3719.9 | Fe | 1000 | 5 | 4271.8 | Fe | 1000 | 48 |
| 3734.9 | Fe | 1000 | 21 | 4307.9 | Fe | 1000 | 42 |
| 3737.1 | Fe | 1000 | 5 | 4325.8 | Fe | 1000 | 42 |
| 3749.5 | Fe | 1000 | 21 | 4383.6 | Fe | 1000 | 41 |
| 3820.4 | Fe | 800 | 20 | 4404.8 | Fe | 1000 | 41 |
| 3859.9 | Fe | 1000 | 4 | 5269.5 | Fe | 800 | 15 |
| 3886.3 | Fe | 600 | 4 | 5531.4 | | | |
| 3930.3 | Fe | 600 | 4 | to | FeO | | |
| 4063.6 | Fe | 400 | 43 | 6218.9 | | | |

TABLE V.- NEAR-ULTRAVIOLET RADIATION FROM NIKE-CAJUN SOLID IRON METEOR

| Wavelength measured | Wavelength identified | Element | Arc intensity | Multiplet | Wavelength measured | Wavelength identified | Element | Arc intensity | Multiplet |
|---|---|---|---|---|---|---|---|---|---|
| 3440 | 3440.6 | Fe | 500 | 6 | 3864 | 3850.0 | Fe | 500 | 20 |
| | 3441.0 | Fe | 300 | 6 | | 3856.4 | Fe | 500 | 4 |
| 3450 | 3443.9 | Fe | 400 | 6 | | 3859.9 | Fe | 1000 | 4 |
| | 3445.2 | Fe | 300 | 81 | | 3865.5 | Fe | 600 | 20 |
| | 3447.3 | Fe | 100 | 82 | 3888 | 3878.0 | Fe | 400 | 20 |
| | 3450.3 | Fe | 150 | 82 | | 3878.6 | Fe | 300 | 175 |
| | 3451.9 | Fe | 100 | 81 | | 3886.3 | Fe | 600 | 4 |
| | 3452.3 | Fe | 150 | 25 | | 3895.7 | Fe | 700 | 4 |
| 3465 | 3465.9 | Fe | 500 | 6 | 3922 | 3920.3 | Fe | 500 | 4 |
| 3480 | 3475.4 | Fe | 400 | 6 | | 3922.9 | Fe | 600 | 4 |
| | 3476.7 | Fe | 300 | 6 | 3932 | 3927.9 | Fe | 500 | 4 |
| 3490 | 3490.6 | Fe | 400 | 6 | | 3930.3 | Fe | 600 | 4 |
| 3576 | 3570.1 | Fe | 300 | 24 | 4020 | 4021.9 | Fe | 200 | 278 |
| | 3581.2 | Fe | 1000 | 23 | 4041 | 4045.8 | Fe | 400 | 43 |
| 3588 | 3587.0 | Fe | 200 | 23 | 4065 | 4063.6 | Fe | 400 | 43 |
| 3617 | 3618.8 | Fe | 400 | 23 | 4202 | 4202.0 | Fe | 400 | 42 |
| 3630 | 3631.5 | Fe | 500 | 23 | 4260 | 4260.5 | Fe | 400 | 152 |
| 3647 | 3647.8 | Fe | 500 | 23 | 4274 | 4271.2 | Fe | 400 | 152 |
| | 3651.5 | Fe | 300 | 295 | | 4271.8 | Fe | 1000 | 48 |
| 3735 | 3705.6 | Fe | 700 | 5 | | 4282.4 | Fe | 600 | 71 |
| | 3709.3 | Fe | 600 | 21 | 4315 | 4294.1 | Fe | 700 | 41 |
| | 3719.9 | Fe | 1000 | 5 | | 4299.2 | Fe | 500 | 152 |
| | 3722.6 | Fe | 500 | 5 | | 4307.9 | Fe | 1000 | 42 |
| | 3733.3 | Fe | 400 | 5 | | 4315.1 | Fe | 500 | 71 |
| | 3734.9 | Fe | 1000 | 21 | | 4325.8 | Fe | 1000 | 42 |
| | 3737.1 | Fe | 1000 | 5 | 4382 | 4383.6 | Fe | 1000 | 41 |
| | 3745.6 | Fe | 500 | 5 | 4406 | 4404.8 | Fe | 1000 | 41 |
| | 3748.3 | Fe | 500 | 5 | 4412 | 4415.1 | Fe | 600 | 41 |
| | 3749.5 | Fe | 1000 | 21 | 4452 | 4442.3 | Fe | 400 | 68 |
| | 3758.2 | Fe | 700 | 21 | | 4443.2 | Fe | 200 | 350 |
| 3800 | 3795.0 | Fe | 500 | 21 | | 4447.7 | Fe | 200 | 68 |
| | 3797.5 | Fe | 300 | 607 | | 4454.4 | Fe | 200 | 350 |
| | 3798.5 | Fe | 400 | 21 | | 4459.1 | Fe | 400 | 68 |
| | 3799.6 | Fe | 400 | 21 | | 4461.6 | Fe | 300 | 2 |
| 3830 | 3820.4 | Fe | 800 | 20 | | 4466.6 | Fe | 500 | 2 |
| | 3825.9 | Fe | 500 | 20 | 4510 | 4494.6 | Fe | 400 | 68 |
| | 3834.2 | Fe | 400 | 20 | | 4528.6 | Fe | 600 | 68 |
| | | | | | 4700 | 4707.3 | Fe | 100 | 554 |

TABLE VI.- RADIATION FROM NIKE-CAJUN IRON SOLID METEOR RECORDED ON SUPER SCHMIDT SPECTROGRAM

| Wavelength identified | Element | Arc intensity | Multiplet | Wavelength identified | Element | Arc intensity | Multiplet |
|---|---|---|---|---|---|---|---|
| 3859.9 | Fe | 1000 | 4 | 5269.5 | Fe | 800 | 15 |
| 4063.6 | Fe | 400 | 43 | 5531.4 | | | |
| 4307.8 | Fe | 1000 | 42 | to | FeO | | |
| 4404.8 | Fe | 1000 | 41 | 6218.9 | | | |